Available online at www.sciencedirect.com
ScienceDirect
Journal of Pharmaceutical and Biomedical Analysis 44 (2007) 763–772
JOURNAL OF PHARMACEUTICAL AND BIOMEDICAL ANALYSIS
www.elsevier.com/locate/jpba

Structural analysis of photo-degradation in thiazole-containing compounds by LC–MS/MS and NMR

Lianming Wu *, Tricia Y. Hong, Frederick G. Vogt

Analytical Sciences, Chemical Development, GlaxoSmithKline plc., 709 Swedeland Road, King of Prussia, PA 19406, USA

Received 18 January 2007; received in revised form 22 February 2007; accepted 28 February 2007
Available online 4 March 2007

Abstract

The photo-degradation behavior of a pharmaceutical compound previously under development for treatment of overactive bladder was studied. Samples of {4-(4-chloro-3-fluorophenyl)-2-[4-(methyloxy)phenyl]-1,3-thiazol-5-yl} acetic acid were stressed with visible light and were observed to degrade into a single primary photo-degradation product. This unknown product was analyzed by liquid chromatography tandem mass spectrometry (LC–MS/MS) with accurate mass measurement and hydrogen/deuterium exchange to determine its molecular weight and formula, isotope distribution patterns and exchangeable protons, and product ion structures. By comparison of the fragmentation pathways of the protonated and sodiated species, the charge was found to locate in the electron-rich part of the molecule after fragmentation. MS-derived structural information combined with stopped-flow ^{1}H LC-nuclear magnetic resonance (NMR) analysis suggested that the degradation product was 4-chloro-*N*-(4-methoxybenzoyl)-3-fluorobenzamide. This unique photo-degradation product was subsequently isolated using preparative-scale chromatography, and its structure was confirmed using 1D and 2D NMR techniques involving the ^{1}H, ^{13}C, ^{15}N and ^{19}F nuclei. The structure of this product suggests that {4-(4-chloro-3-fluorophenyl)-2-[4-(methyloxy)phenyl]-1,3-thiazol-5-yl} acetic acid has reacted with singlet oxygen ($^{1}\Delta_{g}$) via a [4 + 2] Diels-Alder cycloaddition upon photo-irradiation to cause photo-oxygenation in the solid-state (as is common in solution phase), resulting in an unstable endoperoxide that rearranges to the final degradation product structure. Photo-degradation of a structurally related thiazole, 4-(4-Chlorophenyl)thiazol-2-amine, proceeded via a similar process but in a less reactive manner. However, when exposed to the same conditions, sulfathiazole did not degrade, indicating that this photo-degradation process may only occur for thiazole-containing compounds with specific substituents, such as aryl rings.

Keywords: Stress testing of pharmaceuticals; Photo-oxygenation; Singlet oxygen; [4 + 2] Diels-Alder cycloaddition; Thiazoles; Accurate mass; LC–MS/MS; NMR

1. Introduction

It is well known that drug products may undergo physicochemical degradation during manufacturing and storage. The testing of both drug substance and the final dosage form to understand inherent stability characteristics of a product is an essential part of drug development [1]. Part of this process involves determining the chemical structures of compounds produced during stability or forced degradation testing, to ensure that safety is not compromised by the presence of toxic impurities [2]. Currently, tandem mass spectrometry (MS/MS), in conjunction with high-performance liquid chromatography (HPLC), plays a key role in the rapid, on-line structural elucidation of pharmaceutical degradation products, due to its unparalleled speed, intrinsic sensitivity, and molecular specificity [3–5]. Nuclear magnetic resonance (NMR) spectroscopy also plays a major role in degradation product analysis, particularly when the structure must be confirmed for inclusion in regulatory documents, when response factors are needed to assess safety coverage, or when potentially toxic or mutagenic impurities or degradation products are encountered. Two approaches are usually taken when NMR data is required; in the first, compounds of interested are isolated by preparative LC and analyzed by conventional solution-state NMR using a microprobe. In the second approach, hyphenated techniques such as LC–NMR and solid-phase extraction (LC–SPE–NMR) are used in conjunction with flow-probe analysis [6–8].

Thiazoles are an important class of compounds that possess a wide range of pharmacological activity [9,10]. This importance is reflected by the large number of marketed drugs containing

* Corresponding author. Tel.: +1 610 270 4936; fax: +1 610 270 6608.
E-mail address: lianming.2.wu@gsk.com (L. Wu).

0731-7085/$ – see front matter © 2007 Elsevier B.V. All rights reserved.
doi:10.1016/j.jpba.2007.02.037

the thiazole group, such as the anticonvulsant riluzole, the antiparkinsonian talipexole, the antibacterial sulfathiazole, the antiviral ritonavir [9], and the novel drug substances being developed as the large conductance calcium-activated potassium channel openers for overactive bladder indications [11]. In addition, the thiazole ring has also been widely used in the synthesis of natural products [12], polymers [13], fluorescent dyes [14], and insecticides [15]. Like other conjugated five-membered heterocycles (such as furans, thiophenes, pyrroles, indoles, oxazoles, and imidazoles), thiazoles can undergo photo-oxygenation involving singlet oxygen ($^1\Delta_g$) under photo-irradiation in solution [16] and in the solid state [17]. Although several modes for singlet oxygen reactions have been proposed [18–20], the singlet oxygenation of these systems occurs mainly via [4 + 2] Diels-Alder cycloaddition, leading to unstable endoperoxides which, in addition to the classical transformations of peroxides (reduction, hydrolysis, and deoxygenation), afford characteristic rearranged products depending on the heteroatoms, substitution patterns and experimental conditions.

In this communication, we report the photo-oxygenation behavior of solid {4-(4-chloro-3-fluorophenyl)-2-[4-(methyloxy) phenyl]-1,3-thiazol-5-yl} acetic acid upon photo-irradiation (structure **I** in Fig. 1). This molecule is a pharmaceutically active compound previously under development for the treatment of overactive bladder [11]. LC–MS/MS analysis and accurate mass determinations are used to rapidly identify the major photo-degradation product as 4-chloro-*N*-(4-methoxybenzoyl)-3-fluorobenzamide (**II**), which is most likely formed via a [4 + 2] Diels-Alder cycloaddition as described above. Preparative chromatography was used to isolate the degradation product of interest for 1D and 2D NMR experiments (including ^{15}N NMR) to confirm its structure as **II**. The generality of this photo-degradation mechanism in thiazole-containing drugs is explored by LC–MS analysis of 4-(4-Chlorophenyl)thiazol-2-amine (**III**) and the antibacterial drug sulfathiazole (**IV**) after exposure to similar photo-degradation conditions. The ability to understand the structure of significant photo-degradation products of thiazoles allows for better decision-making and control during the drug development process.

I: $C_{18}H_{13}ClFNO_3S$ (Exact Mass: 377.0289)

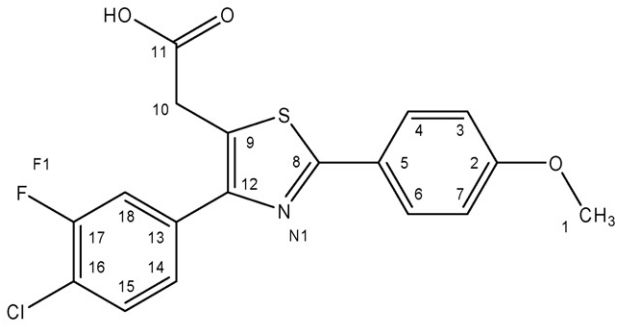

II: $C_{15}H_{11}ClFNO_3$ (Exact mass: 307.0412)

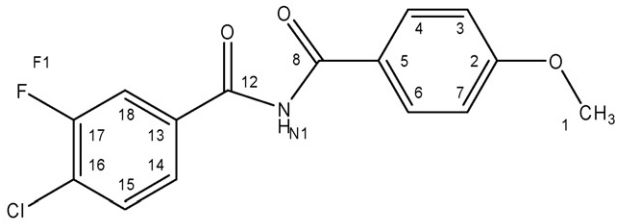

III: $C_9H_7ClN_2S$ (Exact Mass: 210.0018)

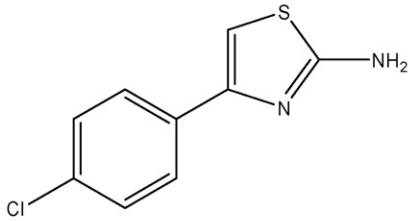

IV: $C_9H_9N_3O_2S_2$ (Exact Mass: 255.0136)

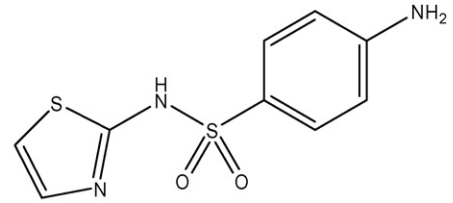

Fig. 1. Structures of the thiazoles examined in this study with their molecular formulae and exact masses. **I**: 4-(4-Chloro-3-fluorophenyl)-2-(4-ethoxyphenyl)-5-thiazole acetic acid (shown with its numbering scheme). **II**: The photo-degradation product of **I**. **III**: 4-(4-Chlorophenyl)thiazol-2-amine. **IV**: Sulfathiazole.

2. Experimental

2.1. Chemicals and reagents

{4-(4-Chloro-3-fluorophenyl)-2-[4-(methyloxy) phenyl]-1,3-thiazol-5-yl} acetic acid was synthesized by GSK. Further discussion of the synthetic preparation of this compound may be found in literature [11]. Samples of 4-(4-Chlorophenyl)thiazol-2-amine and sulfathiazole were purchased from Sigma–Aldrich (Milwaukee, WI, USA).

2.2. LC–MS and LC–MS/MS analysis

Samples were separated on an Agilent 1100 HPLC system (Agilent Technologies, Wilmington, DE, USA). Reversed-phase chromatographic separation was achieved using an Agilent Zorbax SB-Phenyl column (150 mm × 4.6 mm, 3.5 μm particle size) with a mobile phase A of 0.1% formic acid (FA) in water and mobile phase B of 0.1% FA in acetonitrile. The column temperature was kept at 35 °C. The mobile phase composition was linearly ramped to 95% B from 35% B over 10 min with a flow rate of 1 ml/min. UV detection was performed using an Agilent 1100 diode-array detector in the wavelength range of 190–400 nm. For H/D exchange experiments, D_2O was substituted for H_2O in the mobile phase.

The exact mass measurements and MS/MS experiments were performed on a Q-TOF Premier quadrupole orthogonal accel-

eration time-of-flight mass spectrometer with Lockspray™ (Waters Corporation, Manchester, UK) controlled by MassLynx 4.1 software. The electrospray ionization (ESI) source was operated in the positive ion mode with a spray voltage of 3.5 kV, source and desolvation gas temperatures of 120 and 300 °C, an argon collision gas flow rate of 0.45 ml/min in the T-Wave™ guide Mark II collision cell, a collision energy of 30 eV, a desolvation gas flow rate of 600 l/min, and a sample cone voltage of 30 V. The Lockspray™ was operated under identical conditions except with a flow rate at 3 μl/min for infusion of leucine-enkephalin (Leu-Enk). The Q-TOF was calibrated with sodium formate solution at a suitable concentration. All masses were corrected by the internal reference ion with *m/z* 556.2771 (protonated Leu-Enk) that was introduced by the Lockspray™. The atmospheric pressure chemical ionization (APCI) source was operated in the positive ion mode with a corona discharge voltage of 3.0 kV.

2.3. NMR analysis and preparative LC isolation

LC–NMR experiments were performed on a Bruker DRX700 spectrometer (Bruker Instruments, Billerica, MA, USA) with a 3 mm $^{1}H/^{13}C$ SEI flow probe (60 μl active volume) operating at a ^{1}H frequency of 700.13 MHz. An Agilent 1100 (Agilent Technologies) LC was hyphenated to the NMR system via a Bruker HyStar interface, including a Bruker BPSU36-2 peak sampling unit and BMSO column switching unit. An automated on-line Spark-Holland SPE system (Spark, Emmen, The Netherlands) was also used for peak trapping. ^{1}H LC–NMR spectra were obtained in stopped-flow mode with D_2O substituted in the mobile phase and a pre-saturation solvent suppression pulse sequence with a 5 s relaxation delay. Spectra were approximately referenced to the acetonitrile signal at 1.95 ppm. LC–SPE–NMR spectra were obtained in d_3-acetonitrile solution using the basic pulse-and-acquire method with a 10 s relaxation delay.

Samples were isolated for NMR analysis using an Agilent 1100 preparative LC system with an automatic fraction collector (Agilent Technologies). An isocratic method was developed for the preparative isolation of **II** using 45 and 55% of mobile phases A and B, respectively. A Zorbax SB-Phenyl (150 mm × 9.4 mm, 5 μm particle size) column was selected and the flow rate was increased to 4.7 ml/min for the preparative chromatography. The photo-degradation product of interest was observed to elute at a retention time of 15 min (ahead of the major at 20 min) using this isocratic LC method. A loading study was conducted to determine the maximum injection mass; the result was that at a concentration of approximately 5.5 mg/ml, a total of 85 runs each using 700 μl injections were performed, and the fractions combined. Each injection required a 32 min run. The collected fraction was stripped of acetonitrile using a rotary evaporator and was subsequently lyophilized to remove residual water. After isolation, samples were checked using LC–MS. Approximately 2 mg of isolated sample was produced with a purity of about 97% (estimated by LC and solution-state NMR).

NMR experiments on the preparative isolate were also conducted on the DRX700 NMR system using a 5 mm Bruker broadband inverse (BBI) probe with triple-axis gradients. NMR structure elucidation was performed using standard 1D and 2D NMR experiments including ^{13}C spectral editing with the gated spin-echo (GASPE) method, and short and long-range heteronuclear correlation with the heteronuclear single-quantum coherence (HSQC) and heteronuclear multiple-bond coherence (HMBC) experiments [21], respectively. In addition, $^{1}H–^{15}N$ 2D spectra were recorded with heteronuclear multiple-quantum coherence (HMQC) experiments with the *J*-evolution delay set to values ranging from 90 Hz (optimized for one-bond coupling constants) to 1 Hz (optimized for long-range four-bond coupling constants) [21]. ^{19}F 1D spectra were acquired using a Bruker Avance 400 spectrometer equipped with a 5 mm QNI probe using single-pulse experiments with and without ^{1}H broadband decoupling. ^{1}H and ^{13}C NMR spectra were referenced using a small amount of tetramethylsilane added to the samples, while ^{15}N and ^{19}F spectra were externally referenced to nitromethane and $CFCl_3$, respectively.

2.4. Stress testing under exposure to artificial light

Stress testing was carried out according to ICH guidelines for photo-stability testing of drug substances and drug products [22]. The photo-irradiation experiments were performed using a Heraeus Suntest CPS + accelerated exposure testing instrument equipped with a xenon lamp (300–800 nm) with an irradiance of 765 W/m^2 to achieve an exposure equivalent to 2 × ICH conditions.

3. Results and discussion

3.1. MS and MS/MS analysis of the photo-degradation product

3.1.1. Molecular weight and formula determination by accurate mass measurement

Both LC-UV (Fig. 2a) and LC–ESI-MS (Fig. 2b) detected the precursor compound **I** and its photo-degradation product **II** at elution time of 11.4 and 8.6 min, respectively. The extracted ion chromatogram (EIC) of $[\mathbf{I}+H]^+$ at *m/z* 378 (Fig. 2c) confirmed that the peak at 11.4 min corresponded to **I**. Based on the UV peak area, the photo-degradation product **II** accounted for approximately 2% of the photo-degradation sample, in comparison with a control sample. Fig. 3 displays the MS spectrum of this peak, showing the major ions at *m/z* 308, 330 and 637. It is clear that Fig. 3 inserts (a and b) contain one chlorine atom; while Fig. 3 insert (c) has two chlorine atoms. EICs of these three ions suggested that they were all attributable to the same compound. Fragmentation of these three ions is shown in Fig. 4. Since fragmentation of the ion at *m/z* 637 (Fig. 4a) completely gave rise to the ion with *m/z* at 330 by a neutral loss of 307 Da in the MS/MS experiment, it indicates that it is a loosely bound sodiated dimer whose dissociation behavior was extensively studied by the kinetic method [23,24]. In the low *m/z* region in Fig. 3, there is a predominant ion at *m/z* 135, which resulted from the in-source fragmentation as confirmed by EIC of *m/z* 135 and 308 and the MS/MS experiment of the protonated species of the

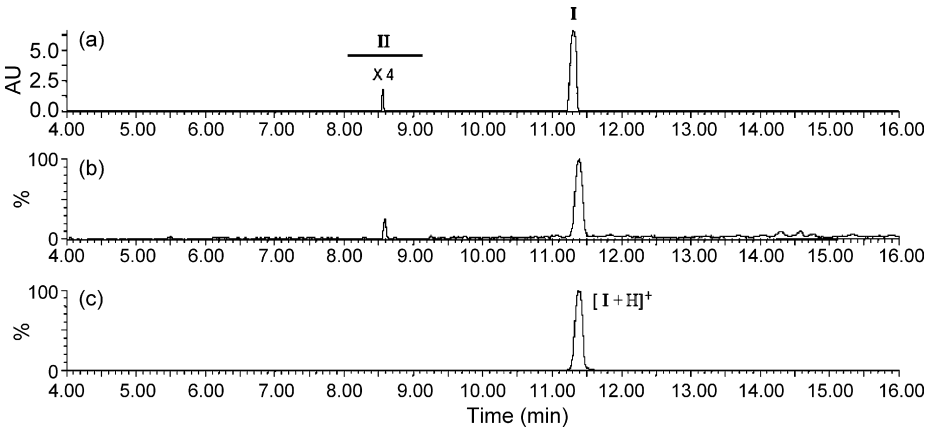

Fig. 2. LC-UV and LC–MS detection of **I** and its photo-degradation product **II**. The UV trace is shown in absorbance units in (a) is the sum of the data between the wavelengths of 190–400 nm. The total ion current (in percent abundance) detected by LC–MS is shown in (b), and the extracted ion chromatogram (EIC) at *m/z* 378 of the protonated molecule of **I** is shown in (c).

degradant at *m/z* 308 (Fig. 4b). From this it was proposed that the degradation product has a nominal mass of 307 Da and the ions at *m/z* 330 and 637 were sodium-bound cluster ions $[M+Na]^+$ and $[2M+Na]^+$, respectively. This proposal is also consistent with the results from H/D exchange experiments using D_2O in the mobile phase, in that both $[M_D+D]^+$ and $[2M_D+Na]^+$ showed an increase of two mass units while $[M_D+Na]^+$ showed an increase of one mass unit. The H/D exchange experiment also confirmed that the unknown photo-degradation product **II** contained one exchangeable hydrogen. The identification of the protonated molecule is further supported by the LC/APCI-MS experiment. The APCI-MS spectrum (not shown) detected only two ions at *m/z* 308 and 135, since sodium-bound cluster ions are not easy to generate by APCI where proton transfer accounted for the main mechanism of ionization of a molecule [25].

The exact mass determination of **II** was based on the mass of both the protonated species $[M+H]^+$ and the sodium adduct $[M+Na]^+$ measured on the Q-TOF MS in full-scan mode. After external lock mass correction, the experimentally determined accurate masses for these ions were 308.0498 and 330.0318 Da, respectively. Using the molecular formula search program in the MassLynx 4.1 software package, the closest match to the molecular formula of the degradation product was found to be $C_{15}H_{11}ClFNO_3$. This elemental composition was concordant with the experimental measurement to within an error of 3.0 ppm.

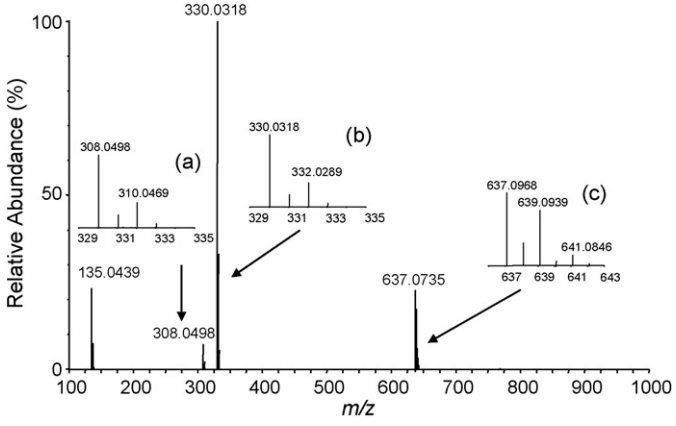

Fig. 3. ESI mass spectrum of compound **II** obtained on the LC peak eluting at 8.6 min (in the gradient method, see Fig. 2). The insets show enlarged regions of the mass spectrum for ions with *m/z* 308 (a), *m/z* 330 (b), and *m/z* 637 (c). These signals are assigned to $[M+H]^+$, $[M+Na]^+$ and $[2M+Na]^+$ ions, respectively.

3.1.2. Structural information obtained by LC–MS/MS with exact mass measurements

In order to facilitate structural elucidation, the MS/MS experiment of the protonated species of the photo-degradation product **II** was studied with exact mass measurements. One of advantages in using the Q-TOF instrument is that it provides structural information such as fragmentation pathways and accurate mass measurements simultaneously, as shown in analysis of carbofuran and its photo-degradation by-products [26]. Fragmentation exclusively gave rise to the product ion at *m/z* 135.0441 (Fig. 4b). This ion was tentatively assigned to an oxonium ion of 4-methoxybenzaldehyde, which could result from an alpha-cleavage of a weak amide bond, indicating that the methoxyphenyl group originally present in **I** is preserved in **II** (as shown in Fig. 5a). The calculated *m/z* for the oxonium ion of 4-methoxybenzaldehyde is 135.0446, which is consistent with the measured value at *m/z* 135.0441 (−3.7 ppm error). Since the precursor did not have an amide bond, this result also implied that photo-irradiation had caused ring-opening of the five-membered thiazole ring and the formation a new amide bond. In addition, the MS data showed one chlorine isotope pattern, suggesting that the chlorinated aromatic ring remained intact in the structure of **II**. By combining this information with the molecular formula determined for **II**, the photo-degradation product was believed to possess a second C=O group. This data, although tentative, was the first to suggest that the photo-degradation of solid **I** had occurred through singlet oxygen ($^1O_2$) [4 + 2] addition followed by rearrangement to produce the photo-degradation product (Fig. 6).

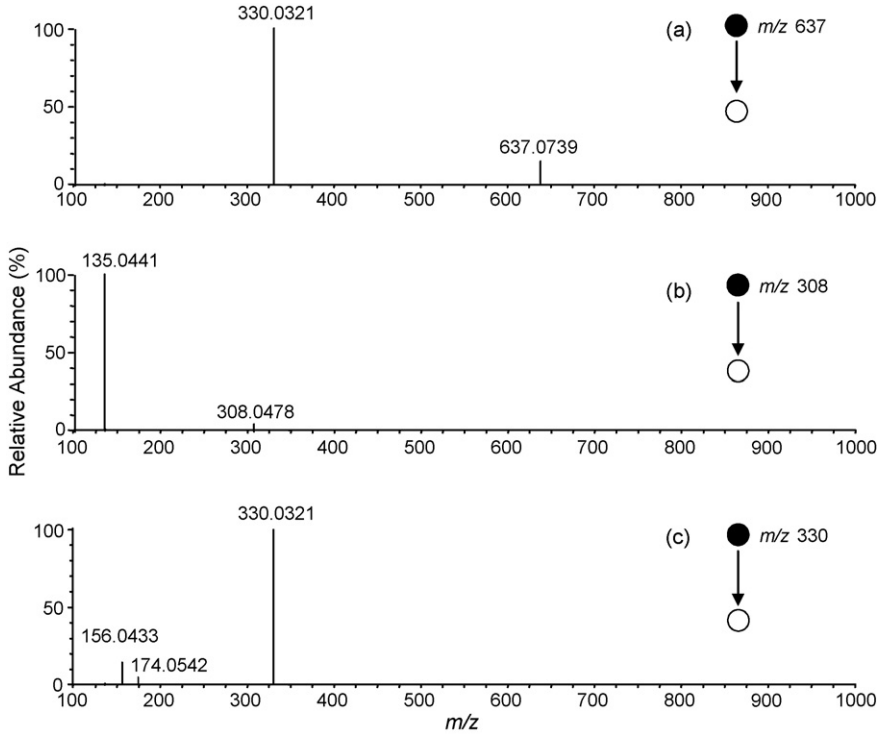

Fig. 4. LC–MS/MS spectra of ions corresponding to **II** at: (a) *m/z* 637; (b) *m/z* 308; (c) *m/z* 330. (See Fig. 3.)

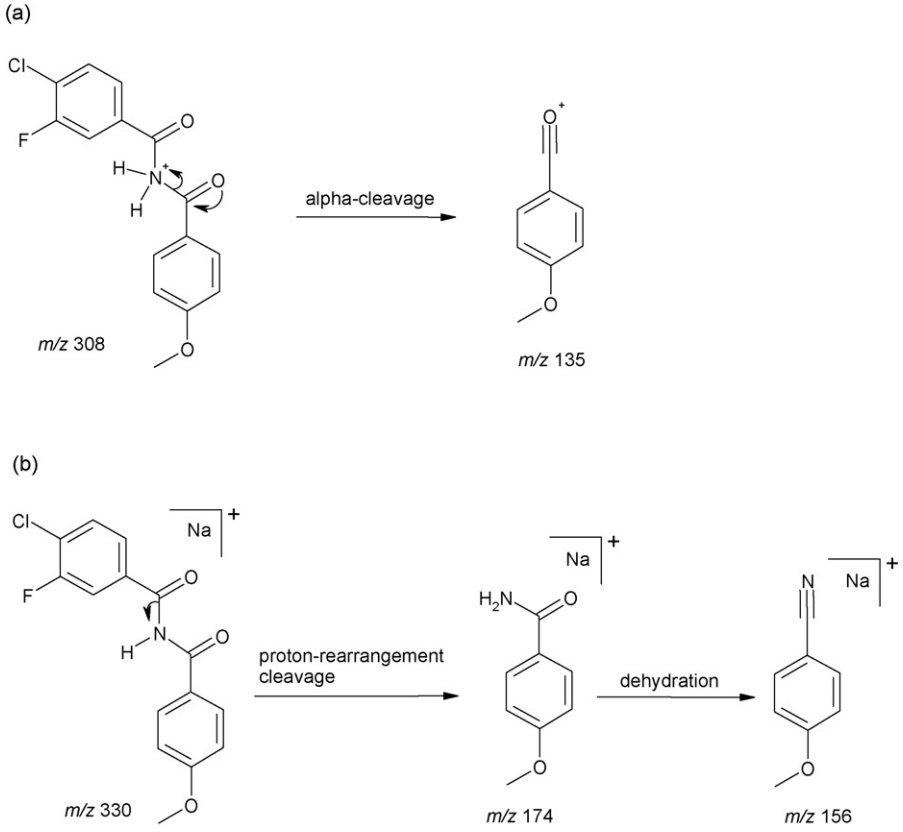

Fig. 5. (a) MS/MS fragmentation pathway proposed for the protonated molecule of **II** at *m/z* 308. (b) MS/MS fragmentation pathway proposed for the sodiated species of **II** at *m/z* 330.

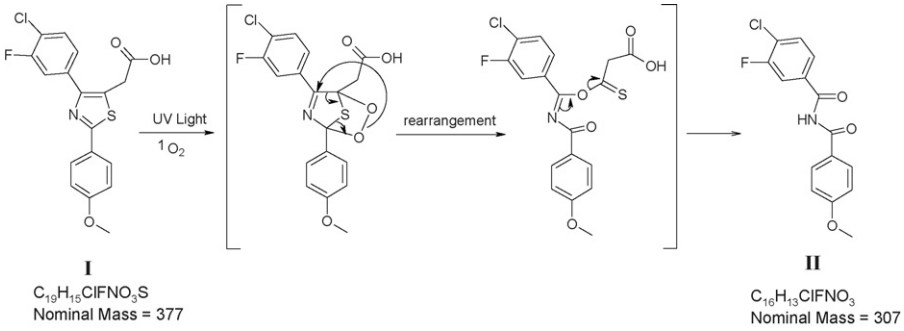

Fig. 6. Proposed photo-degradation process for **I** via singlet photo-oxygenation to **II**.

3.1.3. Comparison of fragmentation pathways of protonated and sodiated species of the degradant

Since MS/MS generally provides indirect structural information of a molecule based on partial structures of product ions, it is useful to obtain more confirmative structural information before reverting to more time-consuming methods such as NMR. In ESI, it is common that both the protonated species and the sodium adduct can be formed. However, their fragmentation pathways are normally different, and examination of the differences can provide useful cross-check information about unknown structures. Therefore, a further MS/MS experiment on the sodium adduct of **II** was performed to determine whether further support could be obtained for the proposed structure.

For the protonated molecule of **II**, it is interesting to observe that one product ion is formed exclusively by the alpha-cleavage of one amide bond but not the other (Fig. 4b). However, when carefully examining the electron density properties of the precursor molecule, it is apparent that the methoxyphenyl ring has one electron donating methoxy group and the fluorochlorophenyl ring has two strong electron-withdrawing groups. The electron-rich part would be expected to stabilize the product ion by delocalizing the charge in the oxonium ion (Fig. 5a). Therefore, the fragmentation pathway of the protonated species supports the proposed structure of **II**.

Fig. 4c shows the MS/MS spectrum of the sodium adduct of **II**. As a metal cation, sodium can chelate with nitrogen and one oxygen in the carbonyl group connected to the methoxyphenyl ring, forming a stable sodium-bound cluster (adduct) ion (Fig. 5b) [24]. Similar to the fragmentation of the protonated molecule, the charge remains in the electron-rich portion of **II** after a proton-rearrangement cleavage, giving rise to one of the product ions at *m/z* 174.0542. This product ion underwent further dehydration by the loss of a molecule of H_2O to form a nitrile which showed the sodium adduct at *m/z* 156.0433. Therefore, fragmentation of the sodiated species also supports the proposed structure of **II**.

3.2. NMR analysis

After the initial MS results, efforts to confirm the proposed structure of **II** first centered on LC–NMR experiments. Stopped-flow LC–NMR is typically a very rapid approach to impurity and degradation product identification in drug development; however, in practice only sensitive nuclei (such as ^1H and ^{19}F) can be studied with this approach [27,28]. Stopped-flow experiments with solvent suppression of both CH_3CN and residual water yielded spectra consistent with the proposed structure of **II**. In particular, the signal from the methylene protons at the 10-position was missing from the spectra. The spectrum of **I** otherwise closely resembled that of **I**, in that all other ^1H resonances observed in spectrum of **I** were also present in the spectrum of **II**, and no additional resonances were detected. Three ^1H resonances attributable to the 3-fluoro-4-chlorobenzyl group retained their characteristic *J*-couplings, but were downfield by 0.2–0.3 ppm compared to the ^1H signals in **I**.

Because of the limitations of ^1H data in the present case, attempts were made to use on-line solid-phase extraction to concentrate material for ^{13}C NMR. Generally, multiple trapping experiments on resin or alkane-functionalized cartridges can be used to pre-concentrate compounds for analysis, after which cartridges can be dried and flushed using deuterated solvent in a concentrated band into a flow probe [29]. Two types of cartridge, the HySphere Resin GP and the HySphere C8 (Spark-Holland) were evaluated. However, in the present case, SPE experiments using these phases were unsuccessful in trapping enough material for ^{13}C NMR, presumably because of either poor trapping efficiency or a tendency for the analyte to wash off the cartridge too easily. Instead, preparative LC isolation was found to be a more successful and efficient approach in the present case, since it required about 3 days of system time versus a larger amount of time needed to screen SPE cartridges and conduct multiple traps (which were not successful). Preparative LC was therefore used to isolate about 3 mg of the degradation product for traditional tube-based NMR analysis.

^1H and ^{13}C NMR spectra of the isolated sample were obtained and were fully assigned using a series of 2D experiments. Expanded regions of the assigned ^1H spectra of compounds **I** and **II** are shown in Fig. 7, with assignments given in Table 1. ^1H integrals and ^{13}C multiplicities (C, CH, CH_2, CH_3) as determined by the GASPE experiment were fully consistent with the assignments reported in Table 1. Several features of the ^1H and ^{13}C NMR data are noteworthy. In the ^{13}C spectrum of **II**, two resonances attributable to the amide carbonyl positions were observed at 166.49 and 165.84 ppm. Three-bond correlations were detected between aromatic protons and the respective

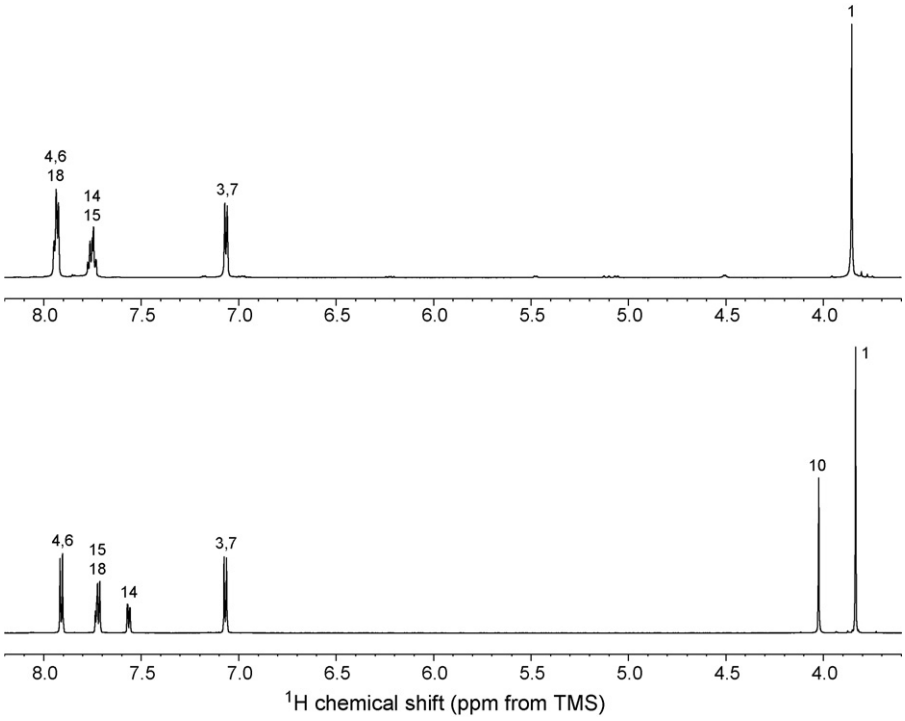

Fig. 7. Comparison of the ^{1}H NMR spectra in d_6-DMSO solution of the parent compound **I** (top) and the preparatively isolated photo-degradation product **II** (bottom). Numbered peaks are in reference to the structures shown in Fig. 1.

amide carbonyls in the ^{1}H–^{13}C heteronuclear multiple-bond coherence experiment. A portion of this HMBC spectrum is depicted in Fig. 8, from which several key aspects of the structure can be readily observed. (The only HMBC correlation not shown in Fig. 8 is that between the protons attached to C1 and C2.) Coupling partners of interest are noted on the spectrum. The ^{1}H and ^{13}C NMR results were thus consistent with the initial structure proposed by MS and ^{1}H LC–NMR experiments. (Although no structural revisions were necessary, it was at least conceivable prior to the full NMR assignment that the C8 and C12 carbonyl groups might have been directly attached to one another, with the amide *ipso*- to one of the aromatic rings. Upon

Table 1
NMR chemical shift assignments and *J*-couplings for **I** and **II** in d_6-DMSO solution[a]

Position	Compound **I**		Compound **II**	
	^{1}H parameters (ppm)	^{13}C, ^{15}N or ^{19}F parameters (ppm)	^{1}H parameters (ppm)	^{13}C, ^{15}N or ^{19}F parameters (ppm)
1	3.83 s	55.31	3.87 s	55.51
2	–	160.98	–	162.93
3/7	7.06 d (J = 8.8 Hz)	114.52	7.18 d (J = 8.7 Hz)	113.62
4/6	7.91 d (J = 8.8 Hz)	127.57	7.93 m	131.00
5	–	125.46	–	125.39
8	–	164.78	–	166.49
9	–	126.64	–	–
10	4.02 s	32.40	–	–
11	12.94 s	171.20	–	–
12	–	149.69 (d, $^{4}J_{C12,F1}$ = 1.7 Hz)	–	165.84 (d, $^{4}J_{C12,F1}$ = 2.0 Hz)
13	–	135.35 (d, $^{3}J_{C13,F1}$ = 7.5 Hz)	–	134.99 (d, $^{3}J_{C13,F1}$ = 6.1 Hz)
14	7.56 dd (J = 8.4, 2.2 Hz)	125.41 (d, $^{4}J_{C14,F1}$ = 3.4 Hz)	7.77 m	125.74 (d, $^{4}J_{C14,F1}$ = 3.3 Hz)
15	7.72 m	130.72 (d, $^{3}J_{C15,F1}$ = 0 Hz)	7.77 m	130.65 (d, $^{3}J_{C15,F1}$ = 0 Hz)
16	–	119.00 (d, $^{2}J_{C17,F1}$ = 17.5 Hz)	–	123.62 (d, $^{2}J_{C17,F1}$ = 17.7 Hz)
17	–	157.05 (d, $^{1}J_{C17,F1}$ = 246.5 Hz)	–	156.73 (d, $^{1}J_{C17,F1}$ = 247.8 Hz)
18	7.72 m	116.41 (d, $^{2}J_{C18,F1}$ = 22.2 Hz)	7.93 m	116.83 (d, $^{2}J_{C18,F1}$ = 22.6 Hz)
N1	–	−68.6[b]	11.28 s	−228.5 (d, $^{1}J_{CN1,NH}$ = 89.8 Hz)[c]
F1	–	−115.74 (dd, J = 10.7, 10.5 Hz)	–	−115.65 (dd, J = 10.2, 9.8 Hz)

[a] Chemical shifts are given in ppm relative to tetramethylsilane (^{1}H and ^{13}C), nitromethane (^{15}N), or $CFCl_3$ (^{19}F). ^{1}H integrals are rounded to the nearest integer. Multiplicity is indicated as s (singlet), d (doublet), t (triplet), q (quartet), or m (multiplet).
[b] Observed via ^{1}H–^{15}N HMQC experiment optimized for 1 Hz *J*-coupling.
[c] Observed via ^{1}H–^{15}N HMQC experiment optimized for 90 Hz *J*-coupling.

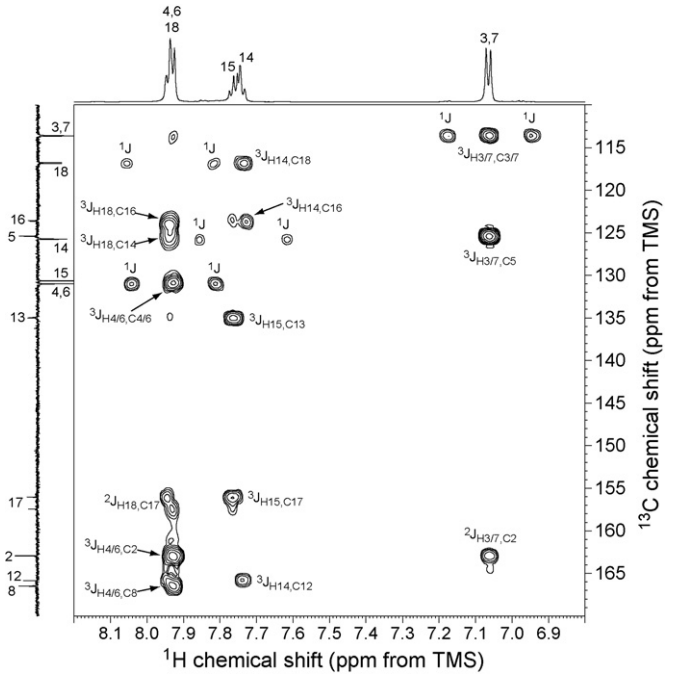

Fig. 8. Expanded region of the 2D ^{1}H–^{13}C HMBC spectrum of compound **II**, shown as a contour plot. Heteronuclear correlations of interest include those involving the C8 and C12 carbonyls ($^{3}J_{H14,C12}$ and $^{3}J_{H4/6,C8}$), which clearly assign these positions. The only correlation not shown in the figure is that between the protons attached to C1 and C2. The 1D ^{13}C multiplicity-edited GASPE spectrum is shown along the F_1 axis and the ^{1}H spectrum is shown along the F_2 axis.

completion of the ^{13}C NMR experiments, these possible structures were ruled out by the lack of a ^{13}C aromatic signal for an aniline, and by the observation of all expected couplings in the HMBC spectrum.)

In addition to the ^{1}H and ^{13}C NMR analysis, ^{19}F spectra of compounds A and B were also obtained on the same samples, resulting in the parameters shown in Table 1. The ^{19}F chemical shifts of **I** and **II** are similar, as expected, and only serve to confirm the presence of aryl fluorine in the degradation product. (However, this is a useful result in itself, as ^{19}F NMR complements the ability of MS to determine the presence of chlorine in the structure of **II**, and LC–NMR can be used to quickly observe its presence.) The shifts are consistent with values reported in the literature for substituted 1-chloro-2-fluorobenzenes [30,31]. A value of −115.9 ppm was reported for 1-chloro-2-fluorobenzene in d_6-DMSO solution, in close agreement with the results in Table 1 [30].

The ^{15}N chemical shifts of compounds **I** and **II** were not determined by direct observation but were measured using inverse-detected 2D HMQC experiments, for sensitivity reasons [32]. Unlike the ^{19}F results, the ^{15}N chemical shifts were highly indicative of the structural change occurring upon photo-degradation. The parent compound **I** exhibited a chemical shift of −68.6 ppm relative to CH_3NO_2 (311.8 ppm relative to ammonia) via the HMQC experiment, in which all four expected ^{4}J ^{1}H–^{15}N correlations were detected. Thiazole rings are known to have highly distinctive ^{15}N chemical shifts; for example, neat liquid thiazole is reported to have a ^{15}N chemical shift of −58.4 ppm [33]. Substitution at the carbon position between the sulfur and the nitrogen can strongly affect the ^{15}N chemical shift (generally causing a shielding trend), as can protonation or formation of a quaternary nitrogen thiazole [30]. Thiazoles with aliphatic carbon substituents between the sulfur and nitrogen are reported to have ^{15}N shifts in the −30 to −70 ppm range, consistent with the value observed for **I** [30]. In contrast, the photo-degradation product **II** has a ^{15}N chemical shift of −228.5 ppm relative to CH_3NO_2 (151.9 ppm relative to ammonia). This chemical shift is indicative of relatively deshielded amide-like nitrogen, which is fully consistent with nitrogen situated between two carbonyl groups. For example, the ^{15}N chemical shift for **II** is similar to the −228 ppm shift reported for phthalimide in d_6-DMSO solution [34], and is also within ∼15 ppm of values reported for phenytoin, aminoglutethimide, phensuximide, salacetamide, and other compounds containing –CONHCO– functional groups [35,36]. It should also be noted that the ^{15}N signal for **II** was detected via a ^{1}H–^{15}N HMQC with a *J*-evolution delay adjusted for 90-Hz coupling constants, so that the experiment also confirmed direct attachment of the nitrogen to the ^{1}H signal at 11.28 ppm. The drastic 180 ppm upfield shift in ^{15}N frequency between **I** and **II** contrasts with the similarity in their ^{1}H and ^{13}C spectra, and highlights the usefulness of including natural-abundance ^{1}H–^{15}N NMR experiments in the analysis of unknown or partially known pharmaceutical compounds [31].

3.3. Generality of photo-degradation reaction of thiazoles

It is proposed that the solid thiazole **I** underwent photo-oxygenation by reacting with singlet oxygen ($^{1}\Delta_g$) upon photo-irradiation as in solution, leading to unstable endoperoxides [16]. However, it is known that in solution, the final characteristic rearranged degradation products depend on the heteroatoms, substitution patterns and experimental conditions. Therefore, an additional photo-irradiation experiment on compound **III** was performed under the same conditions applied to **I**. Based on the reaction mechanism illustrated schematically in Fig. 6, the expected photo-degradation product should have a nominal mass of 198 Da (figure not shown). By LC–MS, EIC of *m/z* 199 ($[M+H]^+$) and 221 ($[M+Na]^+$) showed the presence of a some amount of this degradation product, indicating that 4-(4-Chlorophenyl)thiazol-2-amine could also undergo a similar process (data not shown). Furthermore, other closely related thiazole compounds studied during early-stage development were also observed to undergo the same photo-degradation process by both LC–MS analysis and analysis by preparative isolation and NMR.

The results presented here, although limited to a small number of compounds, suggest that the presence of aromatic substituents on the thiazole ring at the C12 position in **I** and **III** may play a role in the photo-degradation process described here by stabilizing the intermediate depicted in Fig. 6, allowing for the subsequent rearrangement. This was evidenced by another photo-irradiation experiment performed on the antibacterial compound sulfathiazole (**IV**), which possesses a thiazole ring with sulfonamide substituent and no aromatic substituents.

This compound showed no evidence of photo-degradation in the manner of **I** and **III** by LC–MS analysis using two different LC methods and high-sensitivity EIC detection. However, it is believed that the favorable photo-degradation of compound **I** resulted from an intra-molecular proton transfer from the acid group (–COOH) to the nitrogen during rearrangement. In contrast, compound **III** does not possess a carboxylic acid group, and adventitious water might instead be involved in the proton transfer to form the photo-degradation product, causing this compound to be less a reactive participant in this photo-degradation. Further investigation of a wider range of compounds containing the thiazole ring, especially using $^{18}O_2$ gas, is needed to fully understand the structural features necessary for photo-oxygenation.

4. Conclusions

The photo-degradation of solid {4-(4-chloro-3-fluorophenyl) -2-[4-(methyloxy) phenyl]-1,3-thiazol-5-yl} acetic acid was studied by LC–MS/MS and NMR. Because of the somewhat unusual nature of the photo-degradation product, an extensive set of MS and NMR tools was applied to conclusively determine its structure. Based on the structures determined with these techniques, the thiazoles selected in this study are proposed to have reacted with singlet oxygen ($^1\Delta_g$) via [4 + 2] Diels-Alder cycloaddition upon solid-state photo-irradiation to cause photo-oxygenation as in the solution phase, resulting in unstable endoperoxides which lead to the final characteristic rearranged degradation products. A second structurally related thiazole, (4-(4-Chlorophenyl)thiazol-2-amine), exhibited the similar photo-degradation but less reactive behavior. However, a third compound (sulfathiazole) did not degrade in the same manner, suggesting that aromatic substituent groups play a role in this degradation process. As this degradation pathway may represent a significant issue for this class of compounds and might be facilitated by the intra-molecular proton transfer, future investigations will be focused on the photo-degradation behavior of a wider range of five-membered heterocylic compounds, including other thiazole-containing compounds with various substituents, as well as analogs such as oxazoles.

The present work also demonstrates the utility of LC–MS/MS and accurate mass measurements by the Q-TOF instrument in rapidly providing unambiguous structural information for degradation products, including molecular weight and formula, isotope distribution patterns, number of exchangeable hydrogens, and comparison of fragmentation pathways for protonated and sodiated molecules. In the present case, this information allowed the fragmentation patterns to be rationalized and, consequently, the structures of the photo-degradation products to be elucidated; and also allowed for well-supported proposed structures to be intelligently evaluated as necessary using NMR-based analyses. To confirm the structure of **II**, preparative isolation of the photo-degradation product of interest was found to be most efficient approach, as SPE trapping of these compounds was not capable of delivering enough material for the requisite ^{13}C NMR analysis. In addition, the amount of material produced in rapid preparative isolation (when input material quantities of several grams are available) is also sufficient for ^1H–^{15}N NMR analysis, which can offer important structural information beyond that available in ^{13}C experiments when nitrogen atoms are present.

Acknowledgments

The authors acknowledge helpful discussions with Dr. David Q. Liu, Dr. Wengui Wang, Ms. Kaina Jiang, Dr. Sonya Kennedy-Gabb, and Dr. Leo Hsu (GlaxoSmithKline).

References

[1] L. Felton, in: S.W. Baertschi (Ed.), Drug Development and Industrial Pharmacy, vol. 32, 2006, p. 505.
[2] ICH Topic Q1A (R2): Stability Testing of New Drug Substances and Products, Proceedings of the International Conference on Harmonization, EMEA, London, 2003.
[3] D. Breton, D. Buret, A.C. Mendes-Oustric, P. Chaimbault, M. Lafosse, P. Clair, J. Pharm. Biomed. Anal. 41 (2006) 1274–1279.
[4] M. Bakshi, S. Singh, J. Pharm. Biomed. Anal. 34 (2004) 11–18.
[5] X. Xu, M.G. Bartlett, J.T. Stewart, J. Pharm. Biomed. Anal. 26 (2001) 367–377.
[6] C. Pan, F. Liu, Q. Ji, W. Wang, D. Drinkwater, R. Vivilecchia, J. Pharm. Biomed. Anal. 40 (2006) 581–590.
[7] S.X. Peng, Biomed. Chromatogr. 14 (2000) 430–441.
[8] N. Fukutsu, T. Kawasaki, K. Saito, H. Nakazawa, J. Chromatogr. A 1129 (2006) 153–159.
[9] A. Dondoni, A. Marra, Chem. Rev. 104 (2004) 2557–2599.
[10] M.V.N.D. Souza, Eur. J. Sulfur Chem. 15 (2005) 429–449.
[11] M. Hongu, T. Hosaka, T. Kashiwagi, R. Kono, H. Kobayashi, PCT Int. Appl., WO2002/083111 A2 (2002) pp. 1–301.
[12] B. Henkel, B. Beck, B. Westner, B. Mejat, A. Dömling, Tetrahedron Lett. 44 (2003) 8947–8950.
[13] L.Y. Wang, C.X. Zhang, Z.Q. Liu, D.Z. Liao, Z.H. Jiang, S.P. Yan, Inorg. Chem. Commun. 6 (2003) 1255–1258.
[14] V.C. Rucker, S. Foister, C. Melander, P.B. Dervan, J. Am. Chem. Soc. 125 (2003) 1195–1202.
[15] Q. Wang, H. Li, Y. Li, R. Huang, J. Agric. Food Chem. 52 (2004) 1918–1922.
[16] M.R. Iesce, F. Cermola, F. Temussi, Curr. Org. Chem. 9 (2005) 109–139.
[17] M.S.A. Abdou, S. Holdroft, Can. J. Chem. 73 (1995) 1893–1901.
[18] T. Akasaka, W. Ando, in: W. Ando (Ed.), Organic Peroxides, John Wiley, New York, 1992, pp. 599–659.
[19] T. Matsauura, I. Satio, in: O. Buchardt (Ed.), Heterocyclic Compounds, John Wiley, New York, 1976, pp. 456–523.
[20] C.S. Foote, E.L. Clennan, in: C.S. Foote, J.S. Valentine, A. Greenberg, J.F. Liebman (Eds.), Active Oxygen in Chemistry, Chapman & Hall, London, 1995, pp. 105–140.
[21] S. Braun, H.O. Kalinowski, S. Berger, 150 and More Basic NMR Experiments, second ed., Wiley–VCH, New York, 1998.
[22] ICH Topic Q1B, Stability Testing: Photostability Testing of New Drug Substances and Products, Proceedings of the International Conference on Harmonization, EMEA, London, 1996.
[23] R.G. Cooks, J.S. Patrick, T. Kotiaho, S.A. McLuckey, Mass Spectrom. Rev. 13 (1994) 287–339.
[24] L. Wu, E.C. Meurer, B. Young, P. Yang, R.G. Cooks, Int. J. Mass Spectrom. 231 (2004) 103–111.
[25] E.C. Horning, M.G. Horning, D.I. Carroll, I. Dzidic, R.N. Stillwell, Anal. Chem. 45 (1973) 936–943.
[26] A. Detomaso, G. Mascolo, A. Lopez, Rapid Commun. Mass Spectrom. 19 (2005) 2193–2202.
[27] J.C. Lindon, J.K. Nicholson, I.D. Wilson, Prog. NMR Spectrosc. 29 (1996) 1–49.
[28] K. Albert, J. Chromatogr. A 856 (1999) 199–211.

[29] M. Sandvoss, B. Bardsley, T.L. Beck, E. Lee-Smith, S.E. North, P.J. Moore, A.J. Edwards, R.J. Smith, Magn. Reson. Chem. 43 (2005) 762–770.
[30] S. Berger, S. Braun, H.O. Kalinowski, NMR Spectroscopy of the Non-Metallic Elements, Wiley–VCH, New York, 1996.
[31] M.J. Fifolt, S.A. Sojka, R.A. Wolfe, D.S. Hojnicki, J.F. Bieron, F.J. Dinan, J. Org. Chem. 54 (1989) 3019–3023.
[32] G.E. Martin, C.E. Hadden, J. Natl. Prod. 63 (2000) 543–585.
[33] L. Stefaniak, Bull. Acad. Pol. Sci., Ser. Sci. Chim. 26 (1978) 291–302.
[34] M. Bukowska-Strzyzewski, A. Tosik, D. Wodka, J. Zakrzewski, Polyhedron 13 (1994) 1689–1694.
[35] A. Lycka, J. Cizmarik, Pharmazie 43 (1988) 133.
[36] J. Cizmarik, A. Lycka, Pharmazie 43 (1988) 794–795.